Lifetime of the $5d\,^2D_{5/2}$ level of $^{138}Ba^+$ from quantum jumps with single and multiple Ba^+ ions

Elwin A. Dijck,* Amita Mohanty,† Nivedya Valappol, Mayerlin Nuñez Portela,‡ Lorenz Willmann, and Klaus Jungmann
Van Swinderen Institute for Particle Physics and Gravity, Faculty of Science and Engineering, University of Groningen, Zernikelaan 25, 9747 AA Groningen, The Netherlands

(Received 3 July 2017; published 14 March 2018)

The lifetime of the long-lived $5d\,^2D_{5/2}$ level in $^{138}Ba^+$ ions was measured in trapped single ions and small ion crystals using continuous quantum jump spectroscopy. We find $\tau_{D_{5/2}} = 25.6(0.5)$ s, significantly below previously reported values. We have verified our result by exploiting camera images of the stored ions, which enabled monitoring the cleanliness and sufficiently low temperature of the ion samples, and investigating common systematic effects.

DOI: 10.1103/PhysRevA.97.032508

I. INTRODUCTION

Precisely tractable atomic systems render the possibility to measure weak interaction effects. In particular, the weak mixing angle $\sin^2\theta_W$ at the lowest experimentally accessible momentum transfer has been obtained from precision measurements in Cs atoms [1,2]. The extracted value has changed in the recent past by a few standard deviations due to new insights into the theoretical treatment of atomic physics [2]. Heavy alkali-metal atoms such as Fr [3,4] and single trapped heavy alkaline-earth-metal ions such as Ba^+ [5–7] and Ra^+ [8–10] provide unique possibilities to obtain the weak mixing angle more accurately, because weak effects in these systems scale stronger than Z^3, where Z is the nuclear charge [8]. Together with sufficiently accurate and robust calculations of atomic structure to sub-% accuracy, such measurements complement determinations of the weak mixing angle at intermediate and high energies [11]. In some cases they offer the best sensitivity to physics beyond the standard model of particle physics to, among others, particles such as dark Z bosons [12,13] and possible parity-violating cosmic fields [14].

The extraction of standard model parameters from measurements on atomic systems depends crucially on the validity of calculated atomic structure, and particularly on the wave functions. Whereas hyperfine structure and isotope shift measurements scrutinize wave function properties in the vicinity of the nucleus, lifetime measurements provide transition matrix elements and therefore test the long-range parts [8,15,16]. The ions of stable Ba isotopes can be exploited to prepare efficiently for atomic parity violation measurements in Ra^+, which lacks stable isotopes. The latter has closely similar atomic-level structure and experiments are on their way [17]. Lifetime measurements have been performed in various laser-cooled ionic systems with similar long-lived levels stored in rf traps [18–21].

We report here on a series of measurements to determine accurately the $5d\,^2D_{5/2}$ level lifetime in Ba^+. We have scrutinized experimental parameters that could potentially have caused systematic effects.

II. EXPERIMENTAL SETUP

For the experiments, we trap $^{138}Ba^+$ ions in a Paul trap. The electrode surfaces facing the ions are hyperbolically shaped and made from oxygen-free high thermal conductivity copper, mounted to a MACOR holder. The 5-mm-thick ring electrode has an inner diameter of 5 mm and the tips of the two 8-mm-diameter end-cap electrodes are spaced apart 3.5 mm. The trap is operated at rf frequency 6.5 MHz with a voltage amplitude $V_{\rm rf}$ between 100 V and 2500 V applied to the ring. The end caps can be individually biased with dc voltages $V_{\rm bias}$ of order ± 50 mV with respect to ground to minimize ion micromotion (see Fig. 1).

The trap is mounted in a stainless-steel UHV chamber pumped by an ion pump (Gamma Vacuum TiTan 75S) and periodic use of a Ti sublimation pump (Vacom Subli-Con51) maintaining the residual gas pressure $p < 10^{-10}$ mbar. The trap is loaded with Ba^+ ions by resonantly photoionizing a beam of isotopically enriched (98%) ^{138}Ba atoms with laser light at wavelength 413 nm. The atoms are produced by resistively heating a hollow needle filled with $BaCO_3$ and Zr powder mounted 2 cm from the trap center [22]. The trap is reloaded every couple of hours; the barium oven and photoionization laser are off during the measurements. Laser light at wavelengths of 494 and 650 nm is employed for laser cooling by simultaneously driving the strong $6s\,^2S_{1/2} - 6p\,^2P_{1/2}$ and $5d\,^2D_{3/2} - 6p\,^2P_{1/2}$ transitions, respectively (see Fig. 2). The optical setup and laser frequency stabilization are described in more detail in Ref. [23]. A fiber-coupled light-emitting diode (LED, Thorlabs M455F1) produces light at wavelength 456 nm to weakly drive the $6s\,^2S_{1/2} - 6p\,^2P_{3/2}$ transition. A bandpass filter with 10-nm bandwidth (Thorlabs FB450-10) prevents light from the LED at other wavelengths from reaching the ions.

Doppler cooling of Ba^+ ions is performed with typical detunings from resonance of -50 MHz for the light at

*e.a.dijck@rug.nl
†Present address: School of Physical Sciences, National Institute of Science Education and Research, Bhubaneswar 752050, India.
‡Present address: Laboratorio de Óptica Cuántica, Universidad de los Andes, A.A. 4976, Bogotá D.C., Colombia.

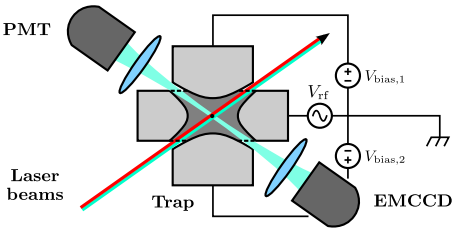

FIG. 1. Schematic view of the hyperbolic Paul trap with rf voltage applied to the ring electrode. Fluorescence from the $6p\,^2P_{1/2} - 6s\,^2S_{1/2}$ transition is detected with a PMT and an EMCCD camera.

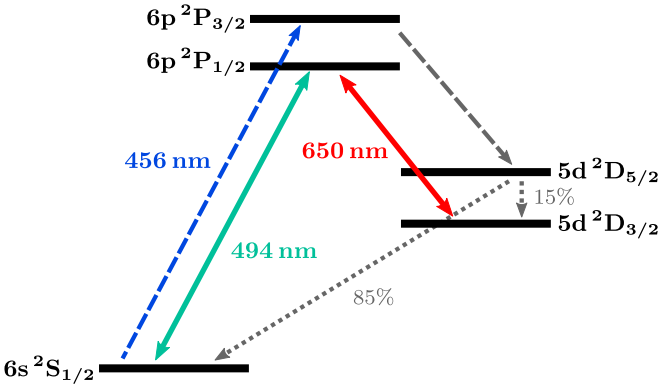

FIG. 2. Energy-level scheme of Ba^+ [24], where $5d\,^2D_{5/2}$ and $5d\,^2D_{3/2}$ are long-lived levels. The ions are laser cooled by exciting the $6s\,^2S_{1/2} - 6p\,^2P_{1/2}$ and $5d\,^2D_{3/2} - 6p\,^2P_{1/2}$ transitions that form a Λ system. Light from an LED at wavelength 456 nm is employed to populate the $5d\,^2D_{5/2}$ level via decay from the $6p\,^2P_{3/2}$ level. The $5d\,^2D_{5/2}$ level decays to either $5d\,^2D_{3/2}$ or the $6s\,^2S_{1/2}$ ground state with a branching ratio of 15% and 85%, respectively [25].

wavelength 494 nm and -2 MHz for the light at 650 nm. The intensity of the light at 494 nm is between 0.1 and 0.6 W/cm^2, and the intensity of the light at 650 nm between 0.1 and 0.7 W/cm^2. The diameter of the laser beams is about 120 μm at the position of the ions in the trap center. We apply a static magnetic field of typically 200 μT to remix dark states [26]. Fluorescence from the $6p\,^2P_{1/2} - 6s\,^2S_{1/2}$ transition is detected with a photomultiplier tube (PMT, Hamamatsu H11123) and with an electron multiplying (EMCCD) camera (Andor iXon DU-897E-CSB-#BB) (see Fig. 1). The photon-counting PMT signal is read out with a time resolution of 100 ms. The positions of the ions in the trap are monitored with submicrometer precision with the EMCCD camera.

III. QUANTUM JUMP SPECTROSCOPY

The lifetime of the $5d\,^2D_{5/2}$ level is directly experimentally accessible by quantum jump spectroscopy (electron shelving [27]) on laser-cooled ions. We perform a continuous measurement, which yields access to the time evolution of the $5d\,^2D_{5/2}$ decay. This is different from the most recent experimental determination in Ref. [25], where the decay probability is probed after a preset wait time, which relies on the accurate knowledge and reproducibility of the probability of state changes. We use light from a high-power LED at wavelength 456 nm to populate the $5d\,^2D_{5/2}$ level via intermediate excitation to the $6p\,^2P_{3/2}$ level (see Fig. 2). Successful shelving into the $5d\,^2D_{5/2}$ level stops fluorescence from the $6p\,^2P_{1/2}$ level. The subsequent reappearance of fluorescence marks the decay of the $5d\,^2D_{5/2}$ level.

The resulting dark and bright periods are analyzed to determine the $5d\,^2D_{5/2}$ level lifetime and the shelving rate, the latter being experimentally controlled by the LED intensity. An example of the PMT count rate versus time for a single Ba^+ ion is shown in Fig. 3. The dark count rate typically is 200 cnt/s and the fluorescence signal 1000 cnt/s per ion at 0.25 W/cm^2 intensity of the light at 494-nm wavelength. For 5% statistical precision on the lifetime $\tau_{D_{5/2}}$, 800 state changes (quantum jumps) are required, corresponding to some 6 h of data taking.

In order to assess the potential effects caused by simultaneously trapped additional ions of the same or also different species, we have performed measurements with ion crystals consisting of up to four ions. As the statistical precision depends on the number of observed state changes limited by the long lifetime of the $5d\,^2D_{5/2}$ level, multiple simultaneously trapped ions provide for higher precision within the same measurement time. Sample data for three ions is shown in Fig. 4. The fluorescence count rate shows four distinct levels, corresponding to zero up to three ions in the dark state at any moment. The EMCCD camera provides a spatially resolved image of bright ions. When any of the ions is shelved into the $5d\,^2D_{5/2}$ level, no change in the position of the remaining bright ions is observed, proving that the dark ions keep their position in the crystal. We set the trapping potential such that ion heating, disappearance of an ion, or joining of an ion of any species would have expressed itself as displacement by several micrometers of the remaining bright-ion positions, which were constantly monitored.

We have collected 68 data sets of typically 2 h length, during which experimental parameters were kept constant. Between data sets, parameters including number of ions trapped, background gas pressure, and laser light intensities were varied to

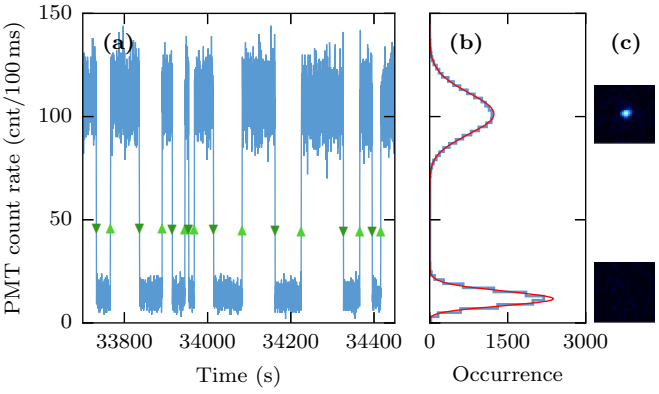

FIG. 3. Example quantum jump data of a single trapped Ba^+ ion. (a) A 12-min recorded trace of fluorescence at 494 nm. Arrows indicate crossing the threshold set in the analysis. (b) Projection of the count rate at 100-ms time resolution showing clear discrimination between the dark and bright state. The peaks are fitted with a model based on Poisson statistics to determine the threshold level. (c) Example EMCCD images of the ion.

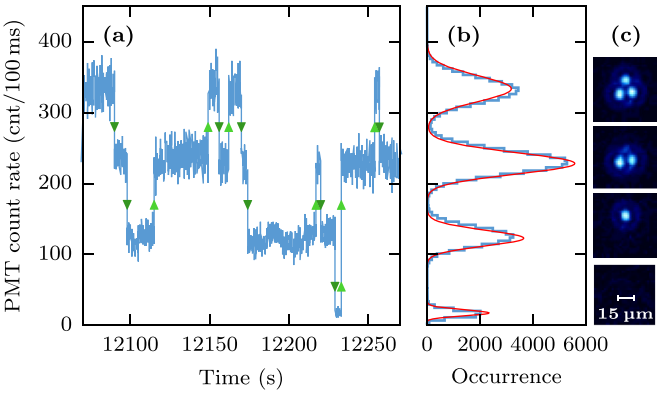

FIG. 4. Example quantum jump data of a three Ba^+ ion crystal. (a) A 3-min recorded trace of fluorescence at 494 nm. Arrows indicate crossing the thresholds set in the analysis. (b) Projection of the count rate at 100-ms time resolution fitted with a model based on Poisson statistics to determine the threshold levels. (c) Example EMCCD images of the ion crystal.

study their influence on the $5d\,^2D_{5/2}$ level lifetime. Experimental parameters were continuously monitored to ensure that only data collected under stable conditions are included in the analysis.

IV. DATA ANALYSIS

Each quantum jump data set is analyzed by an automated procedure that determines the number of ions fluorescing at each point in time by setting thresholds on the PMT count rate (see Figs. 3 and 4). To determine the optimal thresholds, a set of Poisson distributions is fitted to the projection of the count rate [see Figs. 3(b) and 4(b)]. The free parameters are the dark count rate, the increase in count rate per ion, and the peak heights. The count rate with lowest probability between each of the peaks is set as a threshold to discriminate levels. The PMT count rate is averaged over a window of length $\Delta t = 500$ ms to reliably discriminate the dark and bright states for single-ion as well as multiple-ion data sets. Each time the PMT count rate crosses a threshold marks the boundary of an interval [see Figs. 3(a) and 4(a)].

A single-ion data sets consists of two interval types: dark (shelved) and bright (unshelved) periods. The duration distributions of both interval types are determined (see Fig. 5). The dark and bright states correspond to the $5d\,^2D_{5/2}$ level lifetime $\tau_{D_{5/2}}$ and the shelving time τ_S, respectively. In the general case of a measurement with n ions, there are intervals with zero up to n dark ions (see Fig. 6). At each point in time, any fluorescing ion has a constant probability τ_S^{-1} to be excited into the dark state $5d\,^2D_{5/2}$, and any dark ion has a constant probability $\tau_{D_{5/2}}^{-1}$ to decay spontaneously. The effective lifetime τ_k of an interval where k out of n ions are shelved is

$$\tau_k^{-1} = k\tau_{D_{5/2}}^{-1} + (n-k)\tau_S^{-1}. \tag{1}$$

The mean duration of all intervals where k out of n ions are shelved is the maximum likelihood estimate of lifetime τ_k (intervals of some values of k occur more often than others). For data sets with multiple ions, the method of least squares is applied to solve the overdetermined system of equations (1)

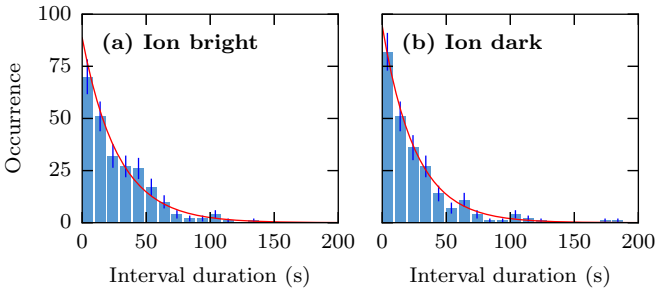

FIG. 5. Example analysis result of the 2-h single-ion data set of Fig. 3. Distribution of dwell times in (a) the bright (unshelved) and (b) the dark (shelved) state. Exponential lifetimes (solid lines) are found by taking the mean of interval durations. After corrections, the mean lifetime of the dark state ($5d\,^2D_{5/2}$ level) is $\tau_{D_{5/2}} = 26.6(1.8)$ s and the mean lifetime of the bright state (shelving time) is $\tau_S = 28.8(2.0)$ s.

for $\tau_{D_{5/2}}$ and τ_S. Averaging the PMT count rate over a time window of length Δt to smooth out noise on short time scales causes short intervals to be missed. A correction of order $2\Delta t$ is applied to correct the exponential lifetimes for this effect (see Appendix A 2).

V. SYSTEMATIC EFFECTS

We have varied several experimental parameters between data sets in order to understand and control systematic effects. The rather long lifetime of the $5d\,^2D_{5/2}$ level in Ba^+ makes it sensitive even to slow processes. We write the observed lifetime as

$$\frac{1}{\tau_{D_{5/2}}} = \frac{1}{\tau_{D_{5/2},\mathrm{nat}}} + \sum_i \gamma_i, \tag{2}$$

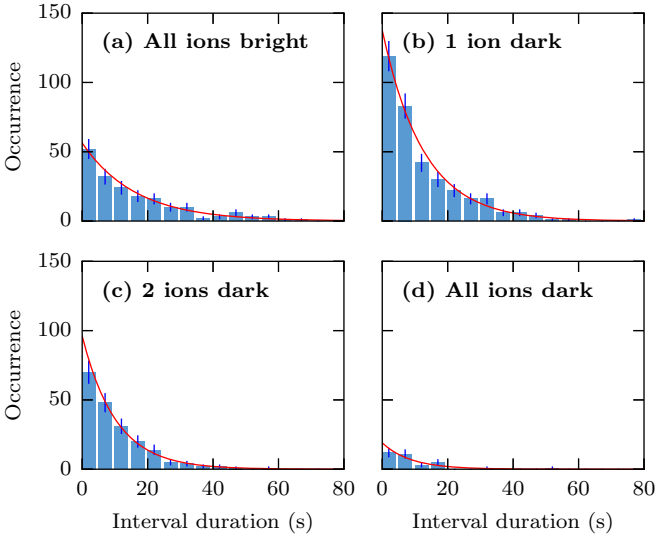

FIG. 6. Example analysis result of the 3-h data set with three ions of Fig. 4. (a)–(d) The distribution of dwell times in the four experimental states with increasing number of ions shelved. The shelving time τ_S and the $5d\,^2D_{5/2}$ level lifetime $\tau_{D_{5/2}}$ are determined from the four time constants τ_k to be $\tau_{D_{5/2}} = 25.6(2.1)$ s and $\tau_S = 50.6(3.9)$ s.

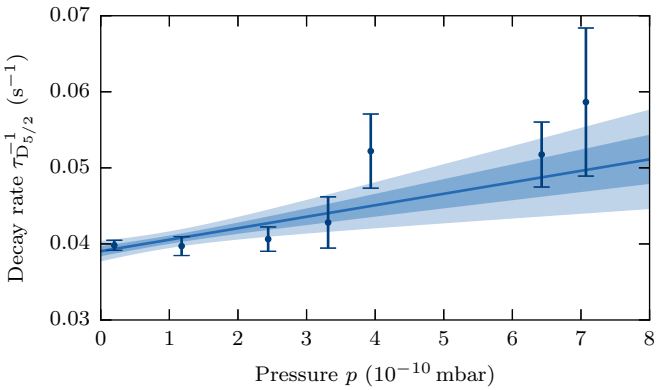

FIG. 7. Extrapolation of the $5d\,^2D_{5/2}$ level decay rate to zero pressure. All single- and multi-ion data sets have been included and grouped for display. (Most data have been collected at the lowest pressure of about 2×10^{-11} mbar.) The fitted quenching rate is $1.5(0.5) \times 10^7$ s^{-1}/mbar, shown with 1σ (standard deviation) and 2σ bounds. The resulting lifetime at zero pressure is 25.6(0.5) s.

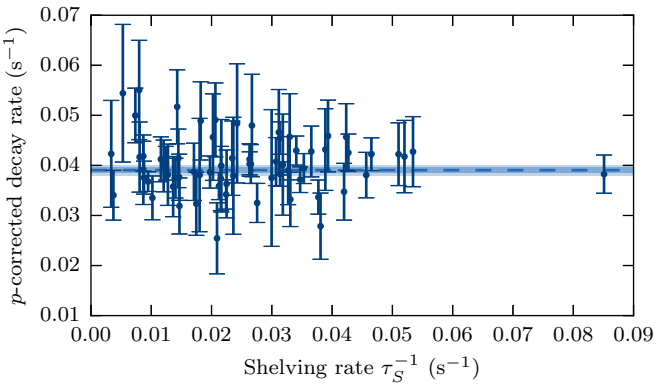

FIG. 8. Decay rate of the $5d\,^2D_{5/2}$ level after subtracting the collisional quenching contribution versus the shelving rate. All data are consistent with the weighted mean, showing no dependence of the lifetime on LED intensity.

where $\tau_{D_{5/2}}$ is the experimentally observed lifetime, $\tau_{D_{5/2},\mathrm{nat}}$ is the natural lifetime, and γ_i are contributions to the decay rate by other processes.

A. Background gas collisions

Collisions with background gas molecules quench the $5d\,^2D_{5/2}$ level [28,29], either to the $5d\,^2D_{3/2}$ level or the ground state (see Appendix B). The quenching rate depends primarily on the pressure and composition of the background gas. The residual gas pressure p was varied between 2×10^{-11} mbar and 7×10^{-10} mbar by reducing the pump speed of the ion pump (see Fig. 7). In a linear least-squares fit of our experimental data, we find a pressure dependence of

$$\gamma_{\mathrm{collision}} = 1.5(0.5) \times 10^7\ \mathrm{s}^{-1} \times p/\mathrm{mbar}, \tag{3}$$

in agreement with previous determinations of this quenching rate [28,29]. Following Eq. (2), we subtract the decay rate $\gamma_{\mathrm{collision}}$ for each data set while investigating further systematic effects (indicated as a pressure-corrected decay rate). Quenching forms the dominant systematic effect in our experiment. The reduced χ-squared value $\chi^2/n = 58.6/66$ of the pressure-correction fit shows that the linear model completely describes our data within statistical uncertainty.

B. Off-resonant scattering

The observed lifetime is affected by excitation out of the $5d\,^2D_{5/2}$ level due to the continuous light from the lasers or the shelving LED [30,31]. The dominant excitation pathway is the $5d\,^2D_{5/2} - 6p\,^2P_{3/2}$ transition at 614 nm. From the transition strength and detuning of the two laser fields, we calculate the deshelving rate (see Appendix C 1):

$$\begin{aligned}\gamma_{\mathrm{lasers}} = {} & 3.0 \times 10^{-6}\ \mathrm{s}^{-1} \times I_{494}/(\mathrm{W/cm^2}) \\ & + 5.9 \times 10^{-5}\ \mathrm{s}^{-1} \times I_{650}/(\mathrm{W/cm^2}),\end{aligned} \tag{4}$$

where I_{494} and I_{650} are the intensities at the position of the ions of the laser light at wavelengths 494 nm and 650 nm, respectively. I_{494} was varied between 0.1 W/cm^2 and 0.6 W/cm^2 and I_{650} between 0.1 W/cm^2 and 0.7 W/cm^2, yielding a negligible contribution to the decay rate of order 10^{-5} s. Additionally, we find no significant ($<1\sigma$) dependence of the pressure-corrected decay rate on either laser light intensity (see Appendix C 1).

The shelving LED at wavelength 456 nm has a broader emission spectrum than the lasers. We estimate its contribution to the deshelving rate from the shelving rate it induces. The total light intensity transmitted through the 10-nm bandwidth of the bandpass filter is about a factor 10^6 larger than the component that drives the $6s\,^2S_{1/2} - 6p\,^2P_{3/2}$ transition. However, the light is far off-resonant from the 614-nm transition, and the resulting suppression yields a deshelving rate of (see Appendix C 2)

$$\gamma_{\mathrm{LED}} \approx 10^{-8} \times \tau_S^{-1}. \tag{5}$$

Varying the intensity of the LED yielded a shelving rate τ_S^{-1} between 0.005 s^{-1} and 0.08 s^{-1}, making the contribution γ_{LED} to the decay rate negligible. We additionally find no significant increase of the pressure-corrected decay rate with the shelving rate (see Fig. 8).

C. Stray electromagnetic fields

The trapped ions are immersed in the black-body radiation field corresponding to the temperature of the surrounding (trap) surfaces. The observed $5d\,^2D_{5/2}$ level lifetime is modified by stimulated emission due to this thermal radiation. While negligible for optical transitions at room temperature, the $5d\,^2D_{5/2} - 5d\,^2D_{3/2}$ transition contributes a deshelving rate of (see Appendix D 1)

$$\gamma_{\mathrm{bb}} = 1.1(0.3) \times 10^{-4}\ \mathrm{s}^{-1}, \tag{6}$$

which effectively shortens the $5d\,^2D_{5/2}$ level lifetime by about 0.1 s. Following Eq. (2), we correct for this effect by subtracting the decay rate γ_{bb} for each data set.

Additionally, ions in the trap experience static electric fields due to patch potentials from material deposited on the electrode surfaces that are not fully compensated. The associated dc Stark effect causes a small degree of mixing of opposite-parity levels that are connected by dipole transitions [31], inducing a finite dipole transition amplitude from the $5d\,^2D_{5/2}$ level

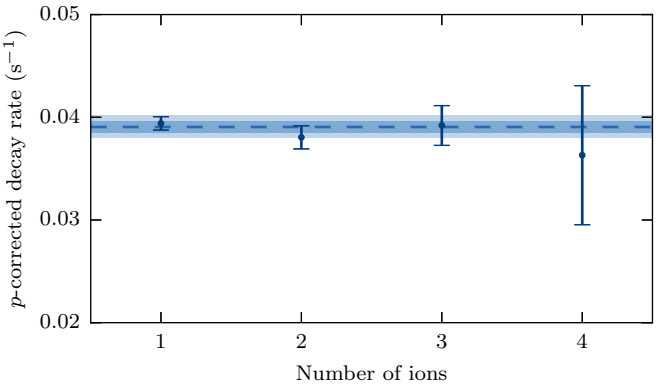

FIG. 9. Pressure-corrected decay rate of the $5d\,^2D_{5/2}$ level as a function of the number of Ba^+ ions of the data set, shown with weighted mean. Most data have been collected with a single ion. No significant difference in the decay rate is found.

to lower levels. Using first-order perturbation theory (see Appendix D 2), we estimate the additional decay rate to be of order

$$\gamma_{\text{Stark}} \approx 10^{-15}\ \text{s}^{-1} \times |E|^2/(\text{V/m})^2, \tag{7}$$

where E is the electric field strength. With observed stray field strengths of no more than 100 V/m in our trap, the shortening of the lifetime of the $5d\,^2D_{5/2}$ level by the Stark effect is negligible.

D. Ion dynamics and interaction

Hot ions that require time for their fluorescence to recover increase the observed lifetime, if during shelving they have left the central fiducial volume and fluorescence at the full level is only achieved after significant cooling. Therefore we have taken care to exclude data sets exhibiting such heating events as unsharp edges of the steps in the fluorescence rate and disturbances to the ion crystal on the EMCCD camera images. The temperature of the ions is influenced by the trapping potential and detuning of the laser frequencies from resonance. In multi-ion measurements, sympathetic cooling is provided by any unshelved Ba^+ ions. We observe no significant dependence of the pressure-corrected decay rate on rf voltage amplitudes or laser detuning (see Appendix E 1).

The temperature of ions also changes through Coulomb interaction with other ions present in the trap, Ba^+ or other. Monitoring the positions of the ions with the EMCCD camera ensures that any change in the number of trapped ions is detected. The typical distance between ions in our experiment is of order 10 μm, and we expect no significant correlation effects (see Appendix E 2). Within statistical precision we find no difference in the pressure-corrected decay rate measured with single ions and ion crystals comprised of up to four Ba^+ ions (see Fig. 9). We combine all data for our final result.

VI. RESULTS AND DISCUSSION

Our final result for $\tau_{D_{5/2}}$ (see Table I) includes a correction for the statistically significant contribution to the decay rate of quenching caused by background gas collisions, a small correction for black-body radiation, and a small correction for bias introduced by the analysis procedure (see Appendix A 3). The results for 1–4 ions are found to be consistent. Combining all data, our measurement of the $5d\,^2D_{5/2}$ level lifetime in Ba^+ is

$$\tau_{D_{5/2}} = 25.6(0.5)\ \text{s}.$$

The result is limited by the statistical precision.

The history of measured and calculated values of the $5d\,^2D_{5/2}$ level lifetime in Ba^+ is compiled in Table II (see also Fig. 10). The theory of the Ba^+ $5d\,^2D_{5/2}$ level lifetime has seen recent activity [16,32]. Most theoretical values seem to lie slightly below the previous measurements. Our result is some 5 standard deviations below the latest independent determination in a different experimental approach [25] and is within 2.5σ of all further previous experimental data. Our result lies >6 standard deviations below the latest calculated values [16,32].

TABLE I. Overview of investigated systematic effects. Corrections to the decay rate are applied using Eq. (2) for all identified effects $\geqslant 10^{-4}\text{s}^{-1}$. The correction for background gas collisions is done by extrapolating the decay rate to zero pressure, since this correction differs per data set. Uncertainties are added in quadrature.

Corrections	Decay rate contribution (s^{-1})
Background gas collisions	$+1.5(0.5)\cdot 10^7 \cdot p/\text{mbar}$
Excitation by 494-nm light	$<10^{-5}$
Excitation by 650-nm light	$<10^{-4}$
Excitation by 456-nm light	$<10^{-5}$
Analysis procedure bias	$-2(2)\cdot 10^{-4}$
Thermal radiation	$+1.1(0.3)\cdot 10^{-4}$
Stray electric fields	$<10^{-5}$
Ion-ion interactions	$<10^{-5}$
Final decay rate	0.0391(7)
Corresponding lifetime $\tau_{D_{5/2}} = 25.6(0.5)$ s	

VII. CONCLUSIONS

We have performed consistent measurements of the $5d\,^2D_{5/2}$ level lifetime in Ba^+, both in single trapped ions and in small crystals of up to four ions. We find a lifetime

TABLE II. Compilation of published values of the lifetime of the $5d\,^2D_{5/2}$ level in Ba^+. For early theory values no uncertainty was given.

Theory			Experiment		
$\tau_{D_{5/2}}$(s)	Year	Ref.	$\tau_{D_{5/2}}$(s)	Year	Ref.
31.09(4)	2018	[32]	25.6(0.5)	2018	This work
30.3(0.5)	2017	[16]	31.2(0.9)	2014	[25]
29.8(0.3)	2012	[15,33]	32.0(2.9)	2007	[34,35]
30.3(0.4)	2010	[36]	32.3(2.6)	1997	[29]
30.3(0.4)	2008	[37]	34.5(3.5)	1990	[28]
31.6	2007	[34]	32(5)	1986	[27]
30.8	2007	[38]	47(16)	1980	[39]
30.3	2001	[40]			

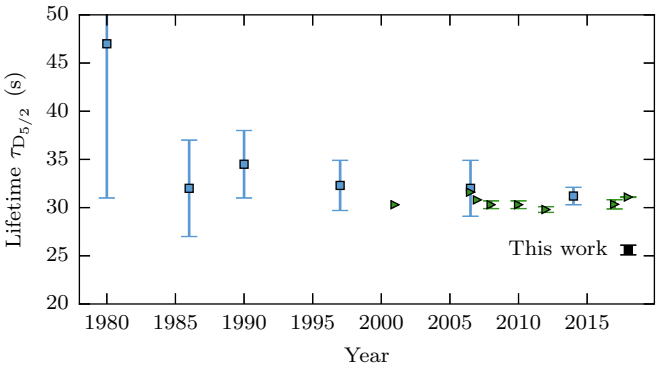

FIG. 10. History of measurements (■) and calculations (►) of the $5d\,^2D_{5/2}$ level lifetime in Ba^+, as listed in Table II.

significantly shorter than previously measured and in disagreement with recent theory (see Table II). We note that the difference between our result and previously published values warrants careful consideration of systematic effects, and we report additional details as Appendices. The sensitivity to finding effects which could affect the measured lifetime was improved by enlarging the probed parameter space and by collecting more statistics. The latter is primarily limited by the required running time due to the rather long $5d\,^2D_{5/2}$ level lifetime in Ba^+. In our experiment, potential artificial prolongation of measured lifetime signals by ion heating has been eliminated through choice of experimental parameters and ion position monitoring. Robust understanding of both atomic theory and experiment is important to support weak mixing angle measurements ahead.

ACKNOWLEDGMENTS

We are grateful to Leo Huisman and Oliver Böll for their technical assistance, and Thomas Meijknecht and Aswin Hofsteenge for helping with data collecting. We acknowledge the financial support from the Dutch foundation FOM under Programme 114 (TRIμP) and Programme 125 (Broken Mirrors and Drifting Constants).

APPENDIX A: LIFETIME EXTRACTION

1. Quantum jump detection

Experimental parameters are kept constant within data sets, and each data set is analyzed separately to investigate systematic effects. The fluorescence rate as a function of time is analyzed by an automated procedure that determines the number of ions fluorescing at each point in time by setting thresholds on the PMT count rate. The thresholds are set to the fluorescence rates of lowest probability between Poisson distributions fitted to the projection of the PMT count rate of each data set, where the free parameters are the dark count rate, the count rate increase per ion, and the peak heights. For this reason, thresholds lie closer to the lower count rate level. Each time the PMT count rate crosses a threshold marks the boundary of an interval.

The mean length of all intervals in a data set where k out of n ions are shelved is the maximum likelihood estimate of the effective exponential lifetime τ_k with uncertainty $\sigma_{\tau_k} = \tau_k/\sqrt{N_k}$, where N_k is the number of samples. These lifetimes τ_k are related to the shelving rate $R_\uparrow = \tau_S^{-1}$ and deshelving rate $R_\downarrow = \tau_{D_{5/2}}^{-1}$ of a single ion:

$$\tau_k^{-1} = kR_\downarrow + (n-k)R_\uparrow = k\tau_{D_{5/2}}^{-1} + (n-k)\tau_S^{-1}. \tag{A1}$$

2. Averaging window correction

To achieve high signal-to-noise in determining the number of fluorescing ions, the PMT count rate is averaged over a window of length $\Delta t = 500$ ms. A finite averaging window means that short intervals are missed and their duration is absorbed into the surrounding intervals. This increases the means of the interval duration distributions τ_k from Eq. (A1) to become [41]

$$\begin{aligned}\tau_k^*(\Delta t) = \Bigg(&- \exp\left[\frac{\Delta t}{\tau_{k-1}}\right] p_{k\uparrow\downarrow}\tau_{k+1} - \exp\left[\frac{\Delta t}{\tau_{k+1}}\right] p_{k\downarrow\uparrow}\tau_{k-1} + \exp\left[\frac{\Delta t}{\tau_{k+1}} + \frac{\Delta t}{\tau_{k-1}}\right] \\ &\times [\tau_k + p_{k\uparrow\downarrow}\tau_{k+1} + p_{k\downarrow\uparrow}\tau_{k-1} - \Delta t(p_{k\uparrow\downarrow} + p_{k\downarrow\uparrow} - 1)]\Bigg) \Bigg/ \Bigg(\exp\left[\frac{\Delta t}{\tau_{k-1}}\right] p_{k\uparrow\downarrow} + \exp\left[\frac{\Delta t}{\tau_{k+1}}\right] p_{k\downarrow\uparrow} \\ &- \exp\left[\frac{\Delta t}{\tau_{k+1}} + \frac{\Delta t}{\tau_{k-1}}\right](p_{k\uparrow\downarrow} + p_{k\downarrow\uparrow} - 1)\Bigg).\end{aligned} \tag{A2}$$

Here $p_{k\uparrow\downarrow} = p_{k\uparrow}p_{(k+1)\downarrow}$ and $p_{k\downarrow\uparrow} = p_{k\downarrow}p_{(k-1)\uparrow}$, with

$$p_{k\downarrow} = \frac{kR_\downarrow}{kR_\downarrow + (n-k)R_\uparrow} \text{ and } p_{k\uparrow} = \frac{(n-k)R_\uparrow}{kR_\downarrow + (n-k)R_\uparrow}.$$

Expression (A2) models the effect of missing any number of short intervals where the number of fluorescing ions k changes by ± 1 within the averaging window length Δt. This covers all possibilities for single-ion ($n = 1$) quantum jump data and forms an adequate approximation for multi-ion data ($n > 1$). Note that when $\Delta t \to 0$, Eq. (A2) reduces to Eq. (A1). The typical magnitude of the correction on the lifetime is of order $2\Delta t$.

For each data set, we numerically solve the system of equations (A2) for $\tau_{D_{5/2}}$ and τ_S using a least-squares fit when $n > 1$ and the system is overdetermined. We have verified this correction by applying an averaging window Δt to pseudo-randomly generated quantum jump data of known $\tau_{D_{5/2}}$ and τ_S (see Fig. 11).

3. Data sets and analysis bias

Experimental parameters and camera images were continuously monitored to ensure that only data collected under stable conditions are included in the analysis. Data sets exhibiting

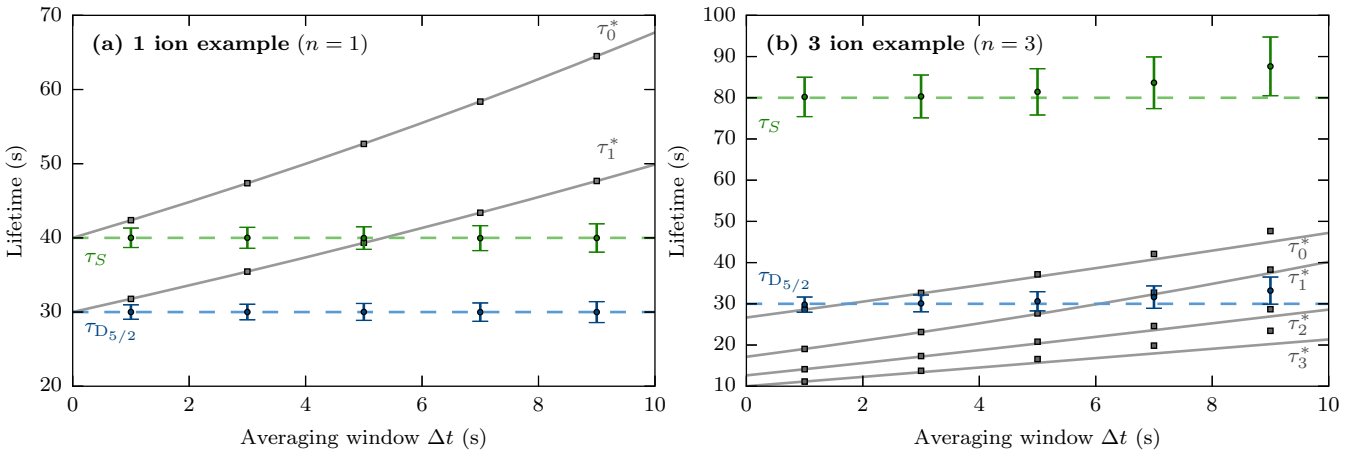

FIG. 11. Testing the averaging window correction with simulated data sets of (a) a single ion, 1000 intervals, $\tau_{D_{5/2}} = 30$ s, $\tau_S = 40$ s; and (b) three ions, 1000 intervals, $\tau_{D_{5/2}} = 30$ s, $\tau_S = 80$ s. Each stack of points shows the mean observed lifetimes τ_k^* (squares) at different averaging window lengths Δt as described by Eq. (A2) (solid lines), and the reconstructed values of $\tau_{D_{5/2}}$ and τ_S with standard deviation (circles), showing good agreement with the true values (dashed lines) up to large averaging window lengths. The reconstructed values differ less than 1% from the true values at $\Delta t = 0.5$ s.

insufficient signal-to-noise to reliably distinguish fluorescence levels, unstable locking of laser frequencies, unstable rf amplitude, or inadequately cooled ions were discarded. We have collected 68 data sets that pass the data quality criteria. Between data sets, parameters including the number of trapped ions, background gas pressure, and laser light intensities were varied to study their influence on the $5d\,^2D_{5/2}$ level lifetime. The data sets were collected over a period of 2 years, during which improvements were made to the vacuum and signal-to-noise.

The typical length of data sets is around 2 h. The finite length of a data set and any interruptions (e.g., to relock a laser) cut off the tail of the (approximately) exponential distributions τ_k^*. We correct for this small effect by subtracting the inverse of the mean uninterrupted duration from each $(\tau_k^*)^{-1}$ before solving for $\tau_{D_{5/2}}$ and τ_S.

Running the complete analysis (with corrections) on pseudorandomly generated data sets with properties (data set lengths, numbers of ions, lifetime, shelving times, PMT signal-to-noise, and pressure dependence) matching those extracted from our experimental data shows a remaining systematic bias in the extracted decay rate of $-1.8 \times 10^{-4}\,\mathrm{s}^{-1}$. This is caused by a combination of estimating the uncertainties in exponential lifetimes from the lifetime values themselves, the finite time resolution of our data acquisition system (100 ms), and the approximations made in the analysis. We correct our result for this shift and take its magnitude as a systematic uncertainty.

APPENDIX B: BACKGROUND GAS COLLISIONS

1. Quenching

Collisions with background gas molecules quench the $5d\,^2D_{5/2}$ level [28,29]. The quenching rate depends on the pressure and composition of the background gas, as well as on the temperature of the ions.

The vacuum chamber with diameter 20 cm and height 25 cm (316L/316LN ESR stainless steel) has been vacuum fired and glass bead blasted. Dry nitrogen was used for venting, and the setup was baked after each venting at a temperature of >120 °C for >48 h. The volume is pumped by a 75 l/s ion pump (Gamma Vacuum TiTan 75S) mounted some 20 cm from the trap on a 100-mm-diameter flange. Additional pumping is provided by periodic use of a Ti sublimation pump (Vacom Subli-Con51). More details on the vacuum system can be found in Refs. [22] and [42]. The pressure was determined by monitoring the ion-pump current, calibrated against a nude UHV Bayard-Alpert–type ion gauge (Granville-Phillips 274023).

The data sets were collected for a residual gas pressure p between 2×10^{-11} mbar and 4×10^{-10} mbar. For a few measurements, the pumping speed of the ion pump was reduced to reach higher pressures around 7×10^{-10} mbar.

The additional decay rate depends linearly on pressure,

$$\gamma_{\mathrm{collision}}(p) = \alpha p,$$

where α is the quenching rate and p is the residual gas pressure. Fitting our experimental data, we find a quenching rate of $\alpha = 1.5(0.5) \times 10^7\,\mathrm{s}^{-1}/\mathrm{mbar}$ in a least-squares fit (see Fig. 12), which is within the range of quenching rates reported by others [28,29].

Following Eq. (2), we subtract the decay rate $\gamma_{\mathrm{collision}}$ for each data set while investigating further systematic effects (indicated as pressure-corrected decay rate), since quenching will turn out to be the dominant effect. This is reflected in the reduced χ-squared value $\chi^2/n = 58.6/66$ of the pressure-correction fit (see Fig. 12), indicating that this linear model completely describes the data and no further statistically significant dependencies of the decay rate on any parameter that was varied are present.

2. Fine-structure mixing

Collisions with background gas molecules also mix fine-structure levels [29,43], producing population transfer from the $5d\,^2D_{5/2}$ to the $5d\,^2D_{3/2}$ level (and vice versa). The effect can be described by two mixing rates γ_{35} and γ_{53} that scale with pressure [43], leading to an equilibrium between the two

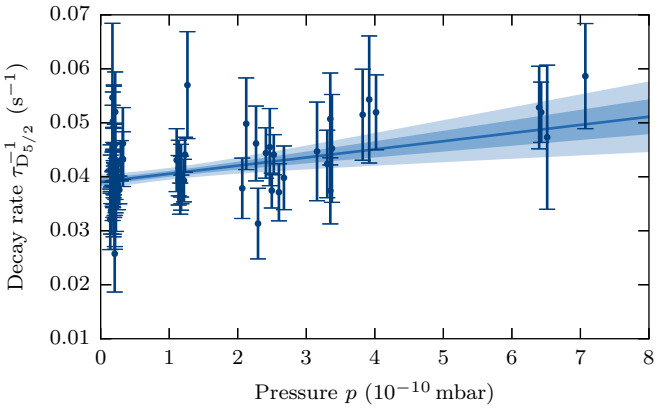

FIG. 12. Extrapolation of the $5d\,^2D_{5/2}$ level decay rate to zero pressure. All single- and multi-ion data sets are included. (Most data have been collected at the lowest pressure of about 2×10^{-11} mbar.) The fitted quenching rate is $1.5(0.5) \times 10^7 \mathrm{s}^{-1}/\mathrm{mbar}$ ($\chi^2/n = 58.6/66$), shown with 1σ (standard deviation) and 2σ bounds. The resulting lifetime at zero pressure is 25.6(0.5) s.

D levels after some time. In general, J mixing is not eliminated by a linear extrapolation to zero pressure. In Ba^+ lifetime measurements where the ions evolve in the dark, J mixing would decrease the observed lifetime of the $5d\,^2D_{3/2}$ level [29] and either increase or decrease the observed lifetime of the $5d\,^2D_{5/2}$ level, depending on mixing rate values. However, in our continuous measurement scheme, the $5d\,^2D_{3/2}$ level is repumped within nanoseconds. This means that in our case, J mixing just forms a contribution to the decay rate term $\gamma_{\mathrm{collision}}$ that scales linearly with pressure and is in fact included in the extrapolation to zero pressure.

APPENDIX C: OFF-RESONANT SCATTERING

1. Laser light at 494 and 650 nm

Excitation out of the $5d\,^2D_{5/2}$ level by continuous radiation from the lasers or the shelving LED affects the lifetime, where the dominant contribution is from excitation of the $5d\,^2D_{5/2} - 6p\,^2P_{3/2}$ transition at 614 nm.

Light at wavelength 494 nm is produced by frequency-doubling light from a Ti:sapphire laser (Coherent MBR-110) in a temperature-tuned MgO:PPLN crystal (Covesion MSHG976-0.5-10). Light at 650 nm is produced by a ring dye laser (Coherent CR-699) operated with DCM dye. Both lasers have a linewidth of about 500 kHz. The laser light is sent to the trapping setup via optical fibers, and the light intensities are controlled by acousto-optic modulators. The frequency stabilization scheme is described in Ref. [23]. The optical setup is described in more detail in Refs. [22] and [42].

The excitation rate R_{12} from a lower level with spin J_1 to a higher level with spin J_2 by laser radiation at angular frequency ω of intensity (irradiance) I_ω is given by [31]

$$R_{12} = \frac{2J_2+1}{2J_1+1}\frac{\pi^2 c^2}{\hbar\omega_{12}^3} A_{21} g(\omega) I_\omega, \tag{C1}$$

where ω_{12} is the atomic resonance frequency, A_{21} is the (partial) spontaneous emission rate from the upper level to the lower level, and $g(\omega)$ is the normalized Lorentzian transition line shape:

$$g(\omega) = \frac{\Gamma/(2\pi)}{(\omega-\omega_{12})^2 + \Gamma^2/4},$$

where Γ is the total width of the upper level. Filling in Eq. (C1) for the two laser fields and the $5d\,^2D_{5/2} - 6p\,^2P_{3/2}$ transition with $\omega_{12} = 2\pi \times 487.99$ THz [24], $A_{21} = 3.4(0.1) \times 10^7 \mathrm{s}^{-1}$ [44], and $\Gamma = 6.32(0.10)$ ns [45] gives the deshelving rate from off-resonant scattering:

$$\gamma_{\mathrm{lasers}}(I_{494}, I_{650}) = 3.0 \times 10^{-6}\mathrm{s}^{-1} \times I_{494}/(\mathrm{W/cm^2}) + 5.9 \times 10^{-5}\mathrm{s}^{-1} \times I_{650}/(\mathrm{W/cm^2}),$$

where I_{494} and I_{650} are the intensities at the position of the ions of the laser light at wavelengths 494 nm and 650 nm, respectively. Contributions by transitions at wavelengths <226 nm to higher-lying P and F levels are smaller by at least 1 order of magnitude. The intensity of the laser light at wavelength 494 nm ranged from 0.1 to 0.6 W/cm^2, and the laser light at 650 nm from 0.1 to 0.7 W/cm^2. The contribution to the decay rate is thus negligible at a level of $10^{-5}\mathrm{s}^{-1}$.

A further possibility would be on-resonant excitation by light at 614 nm from (amplified) spontaneous emission of one of the lasers in addition to its coherent output [30,31]. The gain profile of the DCM dye includes wavelength 614 nm [46]. We have measured the total power of the spontaneous emission of the dye laser to be about 1×10^{-6} times the coherent laser output power. To calculate the induced deshelving rate using Eq. (C1) for a light source that has a much wider spectrum than the atomic transition, we replace the line shape $g(\omega)$ by the spectral function of the spontaneous emission:

$$g = \frac{\Gamma_{\mathrm{DCM}}/(2\pi)}{(\omega_{12}-\omega_{\mathrm{DCM}})^2 + \Gamma_{\mathrm{DCM}}^2/4},$$

where ω_{12} is the angular transition frequency as before, and the emission spectrum of the DCM dye is described by $\omega_{\mathrm{DCM}} \approx 2\pi \times 460$ THz and $\Gamma_{\mathrm{DCM}} \approx 2\pi \times 70$ THz [46]. From the maximum intensity of the coherent laser light at the position of the ions, $I_{650} < 1$ W/cm^2, we find the deshelving rate by (amplified) spontaneous emission to be $<6 \times 10^{-5}\mathrm{s}^{-1}$. The effect is further reduced by at least 1 order of magnitude by a notch filter (Edmund Optics no. 67-111) angled to reflect light at 614 nm placed in the laser beam before reaching the trap. The deshelving rate caused by the spontaneous emission background of the dye laser is thus negligible.

We additionally check our experimental data for a decay rate contribution $\gamma \propto I_\omega$ and find no significant ($<1\sigma$) increase of the pressure-corrected decay rate proportional to either laser light intensity (see Figs. 13 and 14). No correction for laser light intensity is needed.

2. Light at 456 nm

The specifications of the fiber-coupled shelving LED (Thorlabs M455F1) indicate that light emission at wavelength 614 nm is 10^{-5} times less intense than at 456 nm for driving the $6s\,^2S_{1/2} - 6p\,^2P_{3/2}$ transition. Light at 614 nm is further attenuated by the bandpass filter (Thorlabs FB450-10) by a factor 10^{-6}, making on-resonant deshelving negligible. The optical setup is described in more detail in Refs. [22] and [42].

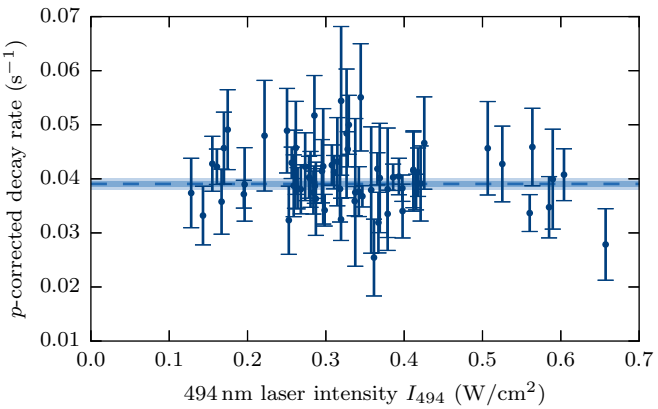

FIG. 13. Pressure-corrected decay rate of the $5d\,^2D_{5/2}$ level as a function of the intensity of the light at 494 nm, with weighted mean, showing no significant dependence.

Comparing the 25 MHz [45] transition linewidth with the 10-nm bandwidth of the filter indicates that the total transmitted light intensity is about a factor 10^6 larger than the component that drives the transition at 456 nm. From the excitation rate τ_S^{-1} induced by the latter component (determined from the quantum jump data) we calculate the off-resonant excitation rate for the transition at 614 nm by the full transmitted spectrum. The transition rate scales as $\Gamma^2/4\Delta\omega^2$ for detunings $\Delta\omega \gg \Gamma$, where Γ is the width of the upper level [see Eq. (C1)], yielding a factor 10^{-14}. Multiplying the two factors (branching ratios and transition strengths are comparable) gives a deshelving rate of order

$$\gamma_{\mathrm{LED}}(\tau_S^{-1}) \approx 10^{-8} \times \tau_S^{-1}.$$

Alternatively, integrating the induced excitation rate at a given intensity for both transitions at 456 nm and 614 nm over the spectrum of the filtered LED [47] yields $\gamma_{\mathrm{LED}} = 1.5 \times 10^{-8} \times \tau_S^{-1}$. This deshelving rate is negligible, since the shelving rate is of the same order as the lifetime $\tau_{D_{5/2}}$.

We additionally check our experimental data for a decay rate contribution $\gamma \propto \tau_S^{-1}$. Varying the LED intensity yielded a shelving rate τ_S between 0.005 and 0.05 s^{-1}. No significant increase of the pressure-corrected $5d\,^2D_{5/2}$ decay rate with the shelving rate is found (see Fig. 8). No correction for LED intensity is needed.

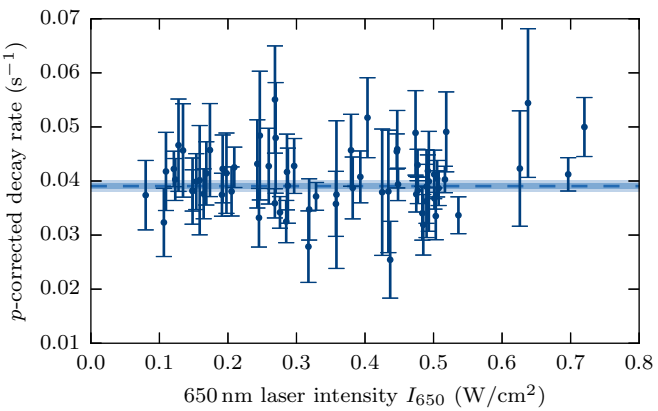

FIG. 14. Pressure-corrected decay rate of the $5d\,^2D_{5/2}$ level as a function of the intensity of the light at 650 nm, with weighted mean, showing no significant dependence.

APPENDIX D: STRAY ELECTROMAGNETIC FIELDS

1. Thermal radiation

The trapped ions are immersed in the black-body radiation field corresponding to the temperature of the surrounding (trap) surfaces. The observed $5d\,^2D_{5/2}$ level lifetime is modified by stimulated emission due to this thermal radiation. The black-body-stimulated emission rate B_{bb} for any electromagnetic transition is related to its spontaneous emission rate A_{21} as [48]

$$B_{\mathrm{bb}}(T) = \frac{A_{21}}{e^{\hbar\omega_{12}/kT} - 1}, \tag{D1}$$

where ω_{12} is its angular transition frequency and T is the temperature of the radiation field. For optical transitions, the effect is generally negligible at room temperature, but the $5d\,^2D_{5/2}$ and $5d\,^2D_{3/2}$ levels in Ba^+ lie fairly close together. The relevant atomic parameters for the $5d\,^2D_{5/2} - 5d\,^2D_{3/2}$ transition are $\omega_{12} = 2\pi \times 24.012$ THz [49] and $A_{21} = 0.0049(8)$ s^{-1} [25]. The deshelving rate due to black-body-stimulated emission at room temperature is thus

$$\gamma_{\mathrm{bb}} = B_{\mathrm{bb}}(300\ \mathrm{K}) = 1.1(0.3) \times 10^{-4}\ \mathrm{s}^{-1},$$

effectively shortening the $5d\,^2D_{5/2}$ level lifetime by about 0.1 s. Following Eq. (2), we correct for this effect by subtracting the decay rate γ_{bb}.

2. Stray electric fields

Charge buildup on the MACOR electrode holder was prevented by applying a grounded thin layer of graphite from a solvent-free pencil to surfaces in direct line of sight to the trap center. Ions in the trap experience static electric fields due to patch potentials from material deposited on the electrode surfaces that are not fully compensated. The associated dc Stark effect causes a small degree of mixing of opposite-parity levels connected by dipole transitions [31].

The interaction Hamiltonian is given by

$$H_{\mathrm{Stark}} = -\vec{D} \cdot \vec{E},$$

where $\vec{D}$ is the electric dipole moment and $\vec{E}$ is the external electric field. This interaction results in a finite electric dipole transition amplitude from the $5d\,^2D_{5/2}$ level to lower levels. Using first-order perturbation theory, the induced decay rate to the $6s\,^2S_{1/2}$ level is given by

$$\gamma_{\mathrm{Stark}} = \frac{8\pi}{3\epsilon_0\hbar\lambda^3} \sum_{m'q} |\langle \widetilde{6\mathrm{S}_{1/2},m'}|D_q|\widetilde{5\mathrm{D}_{5/2},m}\rangle|^2, \tag{D2}$$

summing over all $6s\,^2S_{1/2}$ sublevels m' and polarization states q. The perturbative state corrections are

$$|\widetilde{Jm}\rangle = |Jm\rangle + \sum_{\substack{J'm' \\ \neq Jm}} \frac{\langle J'm'|H_{\mathrm{Stark}}|Jm\rangle}{E_{Jm} - E_{J'm'}} |J'm'\rangle. \tag{D3}$$

Inserting Eq. (D3) into Eq. (D2) and taking into account the selection rules of the dipole operator yields

$$\gamma_{\text{Stark}} = \frac{8\pi}{3\epsilon_0\hbar\lambda^3}\sum_{m'q}\left(\sum_{nm''}\frac{\langle 6S_{1/2},m'|\vec{D}\cdot\vec{E}|nP_{3/2},m''\rangle\langle nP_{3/2},m''|D_q|5D_{5/2},m\rangle}{E_{6S_{1/2}}-E_{nP_{3/2}}} + \sum_{nm''}\frac{\langle 6S_{1/2},m'|D_q|nP_{3/2},m''\rangle\langle nP_{3/2},m''|\vec{D}\cdot\vec{E}|5D_{5/2},m\rangle}{E_{5D_{5/2}}-E_{nP_{3/2}}}\right)^2. \tag{D4}$$

Assuming an isotropic electric field of strength E and filling in the level energies [24] and the dipole transition amplitudes [50] of Ba^+ gives

$$\gamma_{\text{Stark}} = 4\times10^{-15}\ \text{s}^{-1}\times|E|^2/(\text{V/m})^2,$$

which is comparable to the estimate for Ca^+ in Ref. [31]. The induced decay rate from $5d\,^2D_{5/2}$ to $5d\,^2D_{3/2}$ can be calculated the same way, where the sum over intermediate levels includes both P and F levels, but this contribution is several orders of magnitude smaller still.

With observed stray field strengths of no more than 100 V/m in our trap, the shortening of the lifetime of the $5d\,^2D_{5/2}$ level by the Stark effect is negligible, even when taking into account a possible enhancement by up to 3 orders of magnitude due to micromotion [51]. No correction for stray electric fields is therefore needed.

3. Magnetic fields

We apply a static magnetic field of typically 200 μT to remix dark states. The corresponding dc Zeeman effect causes mixing between states; however, the Zeeman effect preserves parity. Thus the Zeeman effect does not affect dipole transition rates analogously to Eq. (D2) and leaves the $5d\,^2D_{5/2}$ lifetime unchanged.

APPENDIX E: ION DYNAMICS

1. Ion temperature

Hot ions that require some time for their fluorescence to recover after shelving alter the observed lifetime. Ions are not laser cooled while shelved in the $5d\,^2D_{5/2}$ level, although they can be sympathetically cooled when multiple ions are trapped and some remain unshelved. If an ion heats up so much that it leaves the central fiducial volume, fluorescence at the full level is only resumed after significant laser cooling. While the actual excitation lifetime is unchanged, this does increase the apparent $5d\,^2D_{5/2}$ lifetime. The heating manifests itself as unsharp edges of the steps in the fluorescence rate and also shows on the EMCCD camera images as disturbances to the ion crystal. We take care to exclude data sets exhibiting such events.

The temperature of the ions is furthermore influenced by the trapping potential and detuning of the cooling laser frequencies from resonance. Data was collected at rf voltage amplitudes V_{rf} ranging from 200 to 800 V (see Fig. 15). The rf signal is generated by a function generator, amplified, then low-pass filtered (Allen Avionics HPLP-11P00-C-300-N) and fed to a resonant circuit ($Q = 76$) to ensure a pure trap drive. The rf amplitude is measured using an rf level meter (Rohde & Schwarz URV35). Additional information on the rf system can be found in Refs. [22] and [42]. No significant dependence of the pressure-corrected decay rate on rf voltage or laser detuning (see Figs. 16 and 17) is observed. Aside from discarding data displaying heating events, we apply no correction for ion temperature.

2. Ion-ion interactions

The temperature of ions changes through Coulomb interaction with other ions present in the trap. Any trapped ions of other species than Ba^+ are not laser cooled and thus contribute

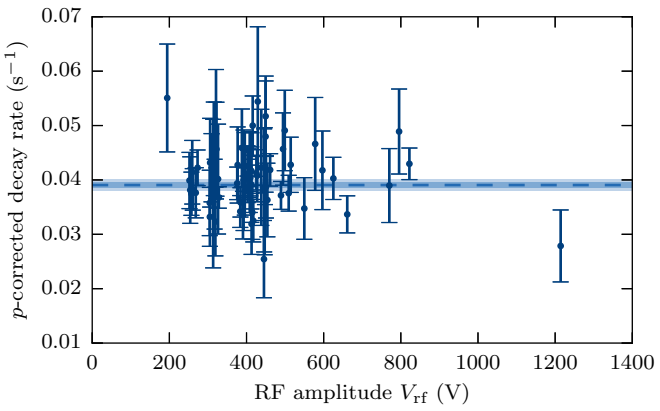

FIG. 15. Pressure-corrected decay rate of the $5d\,^2D_{5/2}$ level as a function of the rf voltage V_{rf}, with weighted mean, showing no significant dependence.

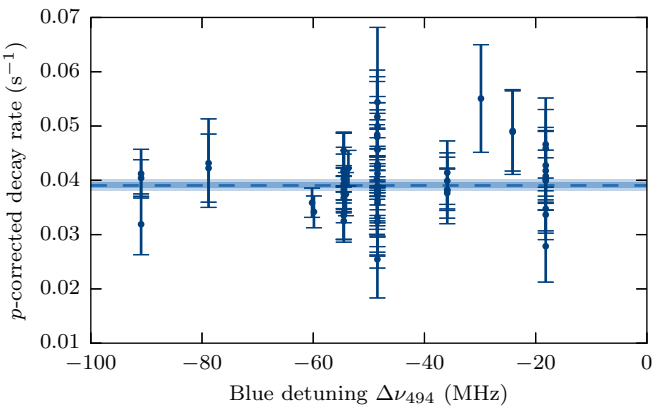

FIG. 16. Pressure-corrected decay rate of the $5d\,^2D_{5/2}$ level as a function of the detuning of the 494-nm laser light $\Delta\nu_{494}$, with weighted mean, showing no significant dependence.

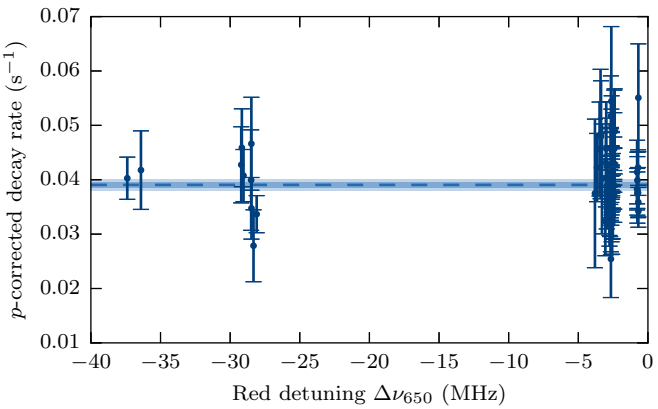

FIG. 17. Pressure-corrected decay rate of the $5d\,^2D_{5/2}$ level as a function of the detuning of the 650-nm laser light $\Delta\nu_{650}$, with weighted mean, showing no significant dependence.

to the heating of the Ba^+ ions. Monitoring the positions of the ions with the EMCCD camera ensures that any change in the number of trapped ions is detected. Within the statistical precision we find no evidence of an effect of additional ions on the pressure-corrected decay rate.

A further effect we consider are correlations in the decay of the $5d\,^2D_{5/2}$ level of multiple Ba^+ ions. The physical mechanism of superradiance and subradiance [52], where the dipole radiation from the spontaneous decay of two or more ions interferes, can produce such correlations. An enhanced rate of multiple jumps (two or more ions shelving or deshelving within the averaging window) was reported in an early experiment with three Ba^+ ions as an indication of cooperative interactions [53]. However, later calculations [54–56] show that the reported enhancement by several orders of magnitude cannot be explained in this way, as the interference effect is limited to deviations of about ±5% from the rates for independent atoms at distances comparable to the wavelength $\lambda = 0.5$ μm and quickly becomes negligible when the distance between the ions becomes larger. Superradiance and subradiance at the level of ±1% has been experimentally observed in the $6p\,^2P_{1/2}$ to $6s\,^2S_{1/2}$ decay rate in a pair of Ba^+ ions separated by about 1.5 μm [57]. In an ensemble of 10 Ca^+ ions, some unexpected double jumps were reported also [30], but subsequent experiments with improved statistics found no correlations or enhanced double or triple jump rates [58–60].

In our experiment, the distance between the ions is typically around 10 μm and we expect cooperative effects to be negligible. We find no significant difference between the pressure-corrected decay rate measured with single ions and measured with ion crystals comprised of up to four Ba^+ ions (see Fig. 9). We combine all data for our final result.

[1] S. C. Bennett and C. E. Wieman, Phys. Rev. Lett. **82**, 2484 (1999).
[2] V. A. Dzuba, J. C. Berengut, V. V. Flambaum, and B. Roberts, Phys. Rev. Lett. **109**, 203003 (2012).
[3] B. K. Sahoo and B. P. Das, Phys. Rev. A **92**, 052511 (2015).
[4] T. Aoki, Y. Torii, B. K. Sahoo, B. P. Das, K. Harada, T. Hayamizu, K. Sakamoto, H. Kawamura, T. Inoue, A. Uchiyama, S. Ito, R. Yoshioka, K. S. Tanaka, M. Itoh, A. Hatakeyama, and Y. Sakemi, Appl. Phys. B **123**, 120 (2017).
[5] N. Fortson, Phys. Rev. Lett. **70**, 2383 (1993).
[6] T. W. Koerber, M. Schacht, W. Nagourney, and E. N. Fortson, J. Phys. B **36**, 637 (2003).
[7] P. K. Panda and B. P. Das, Indian J. Phys. **84**, 817 (2010).
[8] L. W. Wansbeek, B. K. Sahoo, R. G. E. Timmermans, K. Jungmann, B. P. Das, and D. Mukherjee, Phys. Rev. A **78**, 050501(R) (2008).
[9] M. Nuñez Portela, E. A. Dijck, A. Mohanty, H. Bekker, J. E. van den Berg, G. S. Giri, S. Hoekstra, C. J. G. Onderwater, S. Schlesser, R. G. E. Timmermans, O. O. Versolato, L. Willmann, H. W. Wilschut, and K. Jungmann, Appl. Phys. B **114**, 173 (2014).
[10] B. M. Roberts, V. A. Dzuba, and V. V. Flambaum, Phys. Rev. A **88**, 042507 (2013).
[11] C. Patrignani *et al.* (Particle Data Group), Chin. Phys. C **40**, 100001 (2016).
[12] K. S. Kumar, S. Mantry, W. J. Marciano, and P. A. Souder, Annu. Rev. Nucl. Part. Sci. **63**, 237 (2013).
[13] H. Davoudiasl, H.-S. Lee, and W. J. Marciano, Phys. Rev. D **89**, 095006 (2014).
[14] B. M. Roberts, Y. V. Stadnik, V. A. Dzuba, V. V. Flambaum, N. Leefer, and D. Budker, Phys. Rev. D **90**, 096005 (2014).
[15] B. K. Sahoo, R. Chaudhuri, B. P. Das, and D. Mukherjee, Phys. Rev. Lett. **96**, 163003 (2006).
[16] U. I. Safronova, M. S. Safronova, and W. R. Johnson, Phys. Rev. A **95**, 042507 (2017).
[17] L. Willmann, K. Jungmann, N. Severijns, and K. Wendt, Laser Cooling of Ra Ions for Atomic Parity Violation, Report CERN-INTC-2017-069, INTC-I-196 (CERN, 2017), http://cds.cern.ch/record/2266835.
[18] J. C. Bergquist, R. G. Hulet, W. M. Itano, and D. J. Wineland, Phys. Rev. Lett. **57**, 1699 (1986).
[19] N. Yu and L. Maleki, Phys. Rev. A **61**, 022507 (2000).
[20] A. Kreuter, C. Becher, G. P. T. Lancaster, A. B. Mundt, C. Russo, H. Häffner, C. Roos, W. Hänsel, F. Schmidt-Kaler, R. Blatt, and M. S. Safronova, Phys. Rev. A **71**, 032504 (2005).
[21] V. Letchumanan, M. A. Wilson, P. Gill, and A. G. Sinclair, Phys. Rev. A **72**, 012509 (2005).
[22] M. Nuñez Portela, Single ion spectroscopy in preparation of an atomic parity violation measurement in Ra^+, Ph.D. thesis, University of Groningen, 2015.
[23] E. A. Dijck, M. Nuñez Portela, A. T. Grier, K. Jungmann, A. Mohanty, N. Valappol, and L. Willmann, Phys. Rev. A **91**, 060501(R) (2015); Note that switching between two detunings $\Delta\nu_{650}$ at kHz rate was not used for the lifetime measurements.
[24] J. J. Curry, J. Phys. Chem. Ref. Data **33**, 725 (2004).
[25] C. Auchter, T. W. Noel, M. R. Hoffman, S. R. Williams, and B. B. Blinov, Phys. Rev. A **90**, 060501(R) (2014).
[26] D. J. Berkeland and M. G. Boshier, Phys. Rev. A **65**, 033413 (2002).

[27] W. Nagourney, J. Sandberg, and H. Dehmelt, Phys. Rev. Lett. **56**, 2797 (1986).
[28] A. A. Madej and J. D. Sankey, Phys. Rev. A **41**, 2621 (1990).
[29] N. Yu, W. Nagourney, and H. Dehmelt, Phys. Rev. Lett. **78**, 4898 (1997).
[30] M. Block, O. Rehm, P. Seibert, and G. Werth, Eur. Phys. J. D **7**, 461 (1999).
[31] P. A. Barton, C. J. S. Donald, D. M. Lucas, D. A. Stevens, A. M. Steane, and D. N. Stacey, Phys. Rev. A **62**, 032503 (2000).
[32] L. Filippin, S. Schiffmann, J. Dohet-Eraly, D. Baye, and M. Godefroid, Phys. Rev. A **97**, 012506 (2018).
[33] B. K. Sahoo and B. P. Das, Phys. Rev. A **86**, 022506 (2012).
[34] J. Gurell, E. Biémont, K. Blagoev, V. Fivet, P. Lundin, S. Mannervik, L.-O. Norlin, P. Quinet, D. Rostohar, P. Royen, and P. Schef, Phys. Rev. A **75**, 052506 (2007).
[35] P. Royen, J. Gurell, P. Lundin, L.-O. Norlin, and S. Mannervik, Phys. Rev. A **76**, 030502(R) (2007).
[36] U. I. Safronova, Phys. Rev. A **81**, 052506 (2010).
[37] E. Iskrenova-Tchoukova and M. S. Safronova, Phys. Rev. A **78**, 012508 (2008).
[38] C. Guet and W. R. Johnson, Phys. Rev. A **44**, 1531 (1991); **76**, 039905(E) (2007).
[39] F. Plumelle, M. Desaintfuscien, J. L. Duchene, and C. Audoin, Opt. Commun. **34**, 71 (1980).
[40] V. A. Dzuba, V. V. Flambaum, and J. S. M. Ginges, Phys. Rev. A **63**, 062101 (2001).
[41] E. A. Dijck, Ph.D. thesis, University of Groningen (unpublished).
[42] A. Mohanty, Lifetimes, level energies and light shifts in a single trapped Ba^+ ion, Ph.D. thesis, University of Groningen, 2016.
[43] M. Knoop, M. Vedel, and F. Vedel, Phys. Rev. A **52**, 3763 (1995).
[44] N. Kurz, M. R. Dietrich, G. Shu, R. Bowler, J. Salacka, V. Mirgon, and B. B. Blinov, Phys. Rev. A **77**, 060501(R) (2008).
[45] E. H. Pinnington, R. W. Berends, and M. Lumsden, J. Phys. B **28**, 2095 (1995).
[46] E. G. Marason, Opt. Commun. **37**, 56 (1981).
[47] M455F1 and FB450-10 specifications, Thorlabs, Inc.
[48] A. E. Siegman, *Lasers* (University Science Books, Sausalito, CA, 1986).
[49] B. G. Whitford, K. J. Siemsen, A. Madej, and J. D. Sankey, Opt. Lett. **19**, 356 (1994).
[50] J. Kaur, S. Singh, B. Arora, and B. K. Sahoo, Phys. Rev. A **95**, 042501 (2017), Supplemental Material.
[51] D. J. Berkeland, J. D. Miller, J. C. Bergquist, W. M. Itano, and D. J. Wineland, J. Appl. Phys. **83**, 5025 (1998).
[52] R. H. Dicke, Phys. Rev. **93**, 99 (1954).
[53] Th. Sauter, R. Blatt, W. Neuhauser, and P. E. Toschek, Opt. Commun. **60**, 287 (1986).
[54] V. Hannstein and G. C. Hegerfeldt, Phys. Rev. A **68**, 043826 (2003).
[55] V. Hannstein and G. C. Hegerfeldt, Phys. Rev. A **70**, 023820 (2004).
[56] V. Hannstein and G. C. Hegerfeldt, Eur. Phys. J. D **38**, 415 (2006).
[57] R. G. DeVoe and R. G. Brewer, Phys. Rev. Lett. **76**, 2049 (1996).
[58] C. J. S. Donald, D. M. Lucas, P. A. Barton, M. J. McDonnell, J. P. Stacey, D. A. Stevens, D. N. Stacey, and A. M. Steane, Europhys. Lett. **51**, 388 (2000).
[59] M. Knoop, C. Champenois, G. Hagel, M. Houssin, C. Lisowski, M. Vedel, and F. Vedel, Eur. Phys. J. D **29**, 163 (2004).
[60] P. Staanum, I. S. Jensen, R. G. Martinussen, D. Voigt, and M. Drewsen, Phys. Rev. A **69**, 032503 (2004).